

Negative-ion resonances in cross sections for slow-electron–heavy-alkali-metal-atom scattering

C. Bahrim¹ and U. Thumm^{1,2}¹*Department of Physics, Kansas State University, Manhattan, Kansas 66506-2604*²*Fakultät für Physik, Universität Freiburg, D-79104 Freiburg, Germany*

I. I. Fabrikant

Department of Physics and Astronomy, University of Nebraska, Lincoln, Nebraska 68588-0111

(Received 9 December 1999; revised manuscript received 29 November 2000; published 19 March 2001)

We analyze negative-ion resonances in elastic and inelastic total scattering cross sections for slow electron collisions with the heavy-alkali-metal atoms Rb, Cs, and Fr. Our calculations are based on the Dirac R -matrix method [Thumm and Norcross, Phys. Rev. A **45**, 6349 (1992)]. For incident electrons of up to 2.8 eV kinetic energy, we compare a $^3P^o$ shape resonance and $^3P^e$, $^1P^o_1$, and $^1D^o_2$ Feshbach resonances, located below the first excitation threshold of the atomic target in the low-lying spectra of the Rb^- , Cs^- , and Fr^- negative ions, with available experimental data and other calculations. We provide the resonance parameters, partial and converged total elastic and inelastic scattering cross sections, and discuss the relative importance of relativistic effects for the three heavy-alkali-metal targets.

DOI: 10.1103/PhysRevA.63.042710

PACS number(s): 34.80.Bm, 34.80.Dp, 32.10.-f

I. INTRODUCTION

Much experimental and theoretical work has been devoted to the study of the low-lying spectra of atomic and molecular negative ions, and various reviews on this topic are available [1–4]. Negative *alkali-metal* ions are of particular interest because of their simple structure, consisting of two electrons outside a fairly rigid, but polarizable, noble-gas–like core.

In contrast to the long-range Coulomb potential, which can support an infinite number of states in atoms and positive ions, in the short-range potential of negative ions no more than a few bound states can exist. For the negative ions of the alkali-metals, no clear evidence of the presence of bound excited states has been reported. In this paper, we analyze the spectrum of the negative alkali-metal ions Rb^- , Cs^- , and Fr^- by studying the collisions between a projectile electron and a neutral alkali-atom target. The temporary capture of the incident electron in the short-range potential of the target induces a characteristic variation in either elastic or inelastic scattering cross sections, which indicates the presence of a resonance state of the projectile electron-neutral atom system. This phenomenon occurs for particular collision energies E_r . Resonances are commonly classified as either *shape* or *Feshbach* resonances [3]. A *shape* resonance occurs when the projectile electron is temporarily trapped in the potential well resulting from the overlap of the attractive short range potential of the polarized atom and the repulsive centrifugal potential. A *Feshbach* resonance may derive from the potential well associated with an excited state of the target. *Feshbach* resonances often appear when the kinetic energy of the projectile electron is very close to and below an excited state of the atomic target.

For Rb^- and Cs^- , reliable experimental results are available for electron affinities (EA's) [5] and some autoionizing states [3,6–18]. At impact energies below the lowest four atomic excitation thresholds np_j and $(n-1)d_{j'}$ (with $n=5$ for Rb, 6 for Cs, and 7 for Fr, $j=1/2$ and $3/2$, and $j'=3/2$ and $5/2$), accurate electron-atom scattering experiments are

difficult, and up to now only a limited set of measured data for Rb [6–8] and Cs [7–11] targets is available. Close-coupling calculations [19,20] and electron-transmission spectroscopy measurement [6] of total cross sections for Rb targets have suggested the existence of a $^3P^o$ shape resonance below 50 meV. This result was recently confirmed by our relativistic R -matrix calculations [21]. The first evidence in favor of the Cs^- ($^3P^o$) resonance was presented in semi-empirical calculations [22], and confirmed in an analysis of the broadening of Rydberg states by ground-state Cs atoms [23]. Very recently, a single-photon detachment experiment on Cs^- [16] has clearly shown that the Cs^- ($^3P^o$) resonance exists at 8 meV above the detachment threshold, in excellent agreement with detailed Dirac R -matrix calculations [21,24,25]. Our scattering calculations are based on the same Dirac R -matrix method and suggest that the $^3P^o$ state of the Fr^- ion is also unbound [21]. The $^3P^e_2$ fine-structure component was identified in experiments on $e^- + \text{Cs}$ [10], confirming the theoretical R -matrix predictions [24,26].

Additional information about the low-lying photoabsorption spectra of Rb^- and Cs^- ions was obtained in other single and multiphoton detachment experiments. The single-photon detachment technique in a weak laser field was applied for the first time to heavy alkalis in the early 1970's by Patterson *et al.* [12] and was improved later [13–16]. Multiphoton detachment experiments were first realized in the early 1990's. Accurate excess-photon detachment experiments also revealed the $^1P^o_1$ Feshbach resonances in the negative ions of Cs [17] and Rb [18] just below the first np_j atomic excitation threshold. Calculations of the low-energy photoabsorption spectra of Rb^- and Cs^- below the lowest np_j threshold have confirmed these experiments and have predicted similar Feshbach states in the spectrum of Fr^- [27].

The negative ion of Fr is less well studied, and we are aware of only the calculations by Greene [27] for the EA and the photodetachment spectrum below the $6d_{3/2}$ excitation threshold. For neutral Fr, recently published energy levels

and radiative transition probabilities [28], as well as theoretical atomic and core polarizabilities [29,30], provide some of the necessary input for our R -matrix calculations. Based on these data, we have proposed a new value of the EA for Fr [21].

The available data provided by both theory and experiment suggest that the low-lying spectra of different negative alkali-metal ions are similar. This aspect was previously discussed by Johnson and Burrow [7] and by Greene [27]. In a recent paper [21], we investigated $e^- + \text{Rb}$, Cs , and Fr collisions at energies below 120 meV. Together with the above-mentioned $^3P^o$ shape resonance, we have identified a $^3S^e$ virtual state for all three systems.

In the present paper, we will extend the analysis of the low-lying spectra of Rb^- , Cs^- , and Fr^- , for an energy range up to 2.8 eV above the detachment limit (which will serve as the energy reference), with the goal to show that similar resonances compose the low-lying spectrum of all three heavy-alkali negative ions. The $^3P^e$, $^1P^o_1$, and $^1D^o_2$ *Feshbach* resonances below the first np_j atomic excitation thresholds will be identified in both partial and total electron scattering cross sections, and their characteristics (position, shape, and width) will be given and discussed, e.g., with respect to relativistic effects. This paper is structured as follows: in Sec. II, we briefly review the Dirac R -matrix theory and describe our methods for finding and characterizing negative-ion resonances in electron scattering cross sections. In Sec. III, we discuss our results for $e^- + \text{Fr}$ collisions in comparison with our calculations for Rb and Cs targets, and compare the results for Rb and Cs targets with available experimental and theoretical data from the literature. The conclusions follow in Sec. IV. Throughout this paper we will use atomic units, unless stated otherwise.

II. THEORY

Our present calculations are based on the suite of the relativistic Dirac R -matrix programs [24], which provides electron-impact scattering data within a two-electron model. The method was extensively discussed by Thumm and Norcross [24] for $e^- + \text{Cs}$ collisions, and recently applied by Bahrim and Thumm [21] for $e^- + \text{Rb}$ and Fr collisions. Therefore, in the following we shall only give a brief summary of the Dirac R -matrix method and refer to [24] for details. In this model, the two active electrons (the scattered and alkali valence electron) interact with the noble gas-like core through the semiempirical Thomas-Fermi-Dirac-Amaldi potential and a parametric potential which describes the induced polarization of the noble-gas-like core in response to the interaction with an outer electron. We describe the correlation between the two active electrons as the sum of the usual Coulomb interaction and a dielectronic polarization potential V_{diel} which depends on an effective atomic radius R_c adjusted such that the experimental EA is reproduced. The parameters used in our potentials are given in Sec. II of Ref. [21]. In order to provide most accurate values for the position of resonances located very close to the atomic excitation thresholds, our present scattering calculations employ *experimental* excitation thresholds of the neutral atomic target (for

Rb [31], for Cs [31], for Fr [32]), rather than theoretical values as in [24].

Our calculation includes the first five bound states of the target: $ns_{1/2}$, $np_{1/2}$, $np_{3/2}$, $(n-1)d_{3/2}$, $(n-1)d_{5/2}$ (with $n=5$ for Rb , $n=6$ for Cs , and $n=7$ for Fr) and 28 continuum orbitals (COs) in each scattering channel. The lack of completeness in the COs basis set is connected by the inclusion of the Buttler correction [24,33]. The two-electron wave functions are expanded in jj -coupled antisymmetrized products of bound and continuum orbitals for $20 J^\pi$ scattering symmetries and up to 18 channels per scattering symmetry where J and π are the total angular momentum and the parity for $e^- + \text{target}$. A scattering channel is defined as a target state coupled with the spin-orbit angular momentum of the scattered electron to a given J^π symmetry.

A study of the convergence with respect to the inclusion of bound atomic valence states for the low-lying resonances of Cs^- was done by Bartschat [26]. His calculations with five and eight atomic states have shown that no significant contribution to the resonances below the $6p$ excitation threshold results from the addition of higher bound orbitals. In analogy, we expect the inclusion of the five lowest atomic valence orbitals to yield converged results for the low-lying resonances of Rb^- and Fr^- .

The eigenvalues E_k and eigenvectors of the total Hamiltonian inside the R -matrix sphere yield information on possible negative ion states (e.g., the negative ion ground state should be associated with an eigenvector dominated by the ns^2 configuration, with $n=5$ for Rb , 6 for Cs , and 7 for Fr). Our calculations are done within an ‘‘ R -matrix sphere’’ of radius $R=40$ for all three systems. This value is carefully chosen so that the exchange between the projectile and target electrons is negligible outside the sphere. The negative ion states are found by solving the matching equations on the R -matrix sphere. The analysis of partial cross sections and eigenphase sums [defined as $\Delta^{J^\pi}(E) = \sum_{i=1} \tan^{-1}(K_{ii}(E))$], where K_{ii} is the diagonalized open-channel block of the K matrix] in each J^π symmetry on a very fine mesh of scattering energies E allows us to identify resonances. For an isolated resonance the phase shift increases by approximately π radians near the resonance position E_r , and $\Delta^{J^\pi}(E)$ is given as the sum of a slowly varying background phase shift Δ_0 and a strongly energy-dependent resonance term

$$\Delta^{J^\pi}(E) = \Delta_0(E) + \tan^{-1} \left(\frac{\Gamma}{2(E_r - E)} \right), \quad (2.1)$$

where Γ is the resonance width. However, in practice, resonances may overlap or can be strongly influenced by threshold singularities. In such cases Eq. (2.1) does not provide enough accuracy in finding Γ . In order to find reliable estimates for Γ at all energies, we examined both Δ^{J^π} and the partial cross sections in the relevant J^π symmetries. We deduced the position E_r of a resonance from the maximum of the derivative of Δ^{J^π} as a function of E .

We label resonances in the jj -coupling scheme with the set of quantum numbers $(nln'l'; J^\pi)$, where $(nln'l')$ denotes dominant configurations. For practical purposes, it is convenient to also distinguish resonances in the LS -coupling

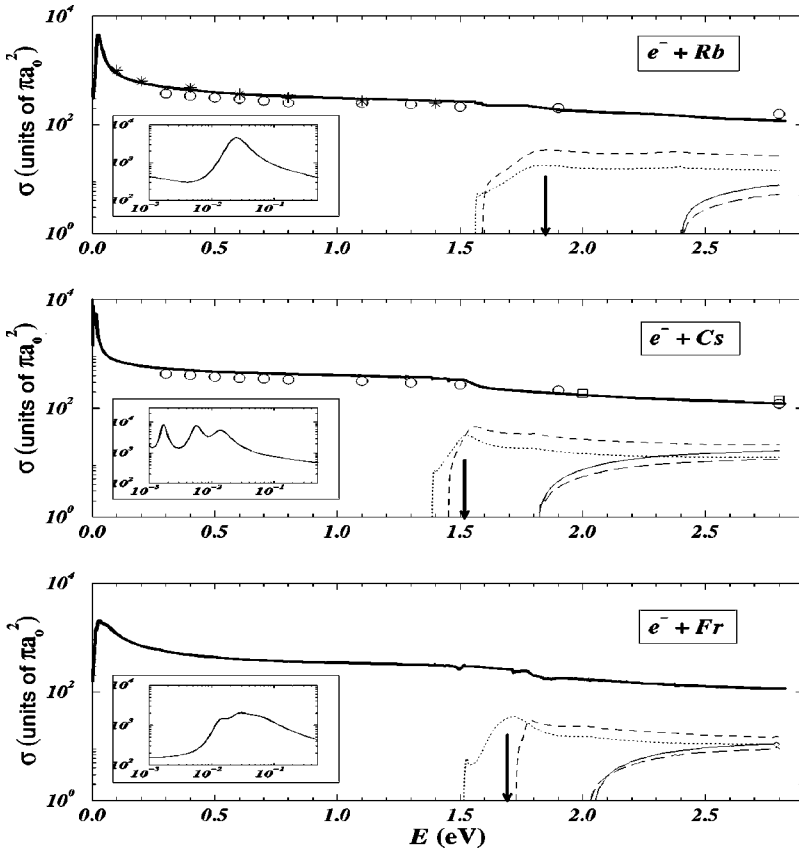


FIG. 1. Total elastic (thick solid line) and inelastic cross sections: $ns_{1/2} \rightarrow np_{1/2}$ (dotted line), $np_{3/2}$ (short dashed line), $(n-1)d_{3/2}$ (long dashed line), and $(n-1)d_{5/2}$ (thin solid line) vs collision energy E for $e^- + \text{Rb}$, Cs, and Fr scattering ($n=5$ for Rb, 6 for Cs, and 7 for Fr). We compare our results with two-state close-coupling calculations [19] (stars) and measured data for $e^- + \text{Rb}$ [8] (circles) and Cs [9] (squares). For both experiments, the size of the symbols indicates the total error in the cross sections. The arrows point to the position of the ${}^3F^o$ resonance. The insets give the elastic cross section for energies below 0.5 eV and show the profile of the ${}^3P^o$ shape resonances.

scheme (where L and S are the total angular momentum and spin quantum numbers of the projectile electron-atom system), especially for excited states optically connected to the ${}^1S_0^o$ ground state of the negative ion (i.e., the ${}^1P_1^o$ Feshbach resonances below the first np excitation threshold).

In order to decide if features observed in the energy dependence of the cross sections are indeed resonances, it is necessary to find some reliable criteria for their identification and correct labeling. Our identification of a particular ${}^3L^\pi$ resonance triplet is primarily based on the analysis of the contribution of configurations to the eigenvectors of the total Hamiltonian inside the R -matrix sphere. For triplet resonances, we search in three subsequent J symmetries of the same parity π for fine-structure components that are dominated by the same $nln'l'$ configurations. For example, the ${}^3P^o$ resonance has to belong to a mixing of $nsn'l'p$ configurations [21]. Next, we solve the matching equations in each relevant J^π symmetry, using a very narrow mesh in collision energy around the eigenvalues associated with the eigenvectors chosen previously. Because the energy splitting between the fine-structure components of the same ${}^3L^\pi$ term is no larger than a few meV, each J component is shifted by about the same amount relative to the corresponding E_k after matching the inner space solutions to the outer space solutions. This is confirmed by our numerical results for all the resonances we analyze in this paper. Finally, we determine whether the splitting between the fine-structure components of the ${}^3L^\pi$ term approximately follows the Landé interval rules [34]

$$\Delta E_r(J, J-1) = E_r(J) - E_r(J-1) = AJ \quad (2.2)$$

and in particular for triplets ($S=1$) with $L \geq S$

$$\Delta E_r(J_{\max}, J_{\min}) = A(2L+1), \quad (2.3)$$

where the Landé constant A characterizes a given triplet. $J_{\max} = L+S$ and $J_{\min} = |L-S|$ are the extremal allowed values for J . In atoms with a single open shell, which is less than half filled, only normally ordered multiplets exist [e.g., for any ${}^3L^\pi$ term we have $E_r(J-1) < E_r(J) < E_r(J+1)$] [34]. Our calculations verify this rule for all ${}^3L^\pi$ multiplets analyzed in this work. In consequence, A is positive.

III. RESULTS AND DISCUSSION

Figure 1 shows the converged total elastic cross section and the total converged inelastic cross sections for the transitions $ns_{1/2} \rightarrow np_{1/2}$, $np_{3/2}$, $(n-1)d_{3/2}$, $(n-1)d_{5/2}$ (with $n=5$ for Rb, $n=6$ for Cs, and $n=7$ for Fr) for collision energies below 2.8 eV. To bring the total cross sections to convergence for such collision energies, we need to include 20 symmetries ($J \leq 9$ and $\pi = \pm 1$) for any of the three targets. For electron scattering by Rb targets at energies below 1.4 eV, Fig. 1 includes the nonrelativistic two-state close-coupling data for elastic cross sections computed by Fabrikant [19], which are in excellent agreement with the present relativistic R -matrix calculations. Absolute total cross sections for electron scattering by Rb and Cs targets were measured by Visconti, Slevin, and Rubin [8] and, more recently, for Cs targets, by Jaduszliwer and Chan [9]. The experimental error of the absolute cross sections is estimated as 15% in

TABLE I. The 3P resonances in Fr^- , labeled in jj - and LS -coupling schemes. Resonance positions E_r and widths Γ , the corresponding R -matrix poles E_k , and the dominant configurations of the associated eigenvector are shown. “ J -av.” stands for our J -averaged energy and width of each resonance. The Landé constant A [defined in Eq. (2.3)] is given in meV.

jj	J^π	Configurations (% probability)	E_k (meV)	E_r (meV)	Γ (meV)	${}^3L^\pi$ (A)
	0^-	$7s7p_{1/2}(37.4)$; $7s8p_{1/2}(37.8)$; $7s9p_{1/2}(20.6)$	11.15	13.21	9.40	${}^3P_0^o$
$7snp$	1^-	$7s7p_{1/2}(20.3)$; $7s8p_{1/2}(27.4)$; $7s9p_{1/2}(19.8)$; $7s8p_{3/2}(11.9)$	21.55	24.02	25.71	${}^3P_1^o$
	2^-	$7s7p_{3/2}(18.4)$; $7s8p_{3/2}(41.3)$; $7s9p_{3/2}(37.2)$	34.88	40.84	68.13	${}^3P_2^o$
	J -av.	$7pn's(n' \geq 7)$		32.16	47.46	${}^3P^o$ (9.2)
	0^+	$7p_{1/2}7p_{1/2}^2(47.5)$; $7p_{1/2}8p_{1/2}(28.4)$; $7p_{3/2}7p_{3/2}(10.5)$	1395.22	1396.42	0.36	${}^3P_0^e$
$7pnp$	1^+	$7p_{1/2}7p_{3/2}(44.9)$; $7p_{1/2}8p_{3/2}(18.1)$; $7p_{3/2}8p_{1/2}(7.5)$	1440.67	1436.48	1.50	${}^3P_1^e$
	2^+	$7p_{3/2}^2(31.7)$; $7p_{1/2}7p_{3/2}(17.3)$; $7p_{1/2}8p_{3/2}(18.1)$; $7p_{1/2}9p_{3/2}(5.4)$; $7p_{3/2}8p_{3/2}(9.8)$; $7p_{3/2}8p_{1/2}(3.4)$	1499.19	1497.81	16.84	${}^3P_2^e$
	J -av.	$7pn'p(n' \geq 7)$		1466.10	9.89	${}^3P^e$ (33.8)

Ref. [8] and about 10% in Ref. [9] and corresponds to the size of the symbols. For collision energies below 1.5 eV, our calculations overestimate the experimental data of Visconti, Slevin, and Rubin [8] by 20%, for both Rb and Cs targets, but reproduce the energy dependence of the experimental electron scattering cross section. This suggests that the statistical error in Ref. [8], estimated at $\pm 6\%$, is in reality twice as large. For collision energies above 1.5 eV, the agreement between our calculations and the two scattering experiments [8,9] is very good.

The structures in our scattering cross sections in Fig. 1 can be related either to the presence of resonances or to threshold effects. The peak close to zero collision energy is due to the ${}^3P^o$ shape resonance. At zero energy we find a large elastic cross section which is due to the large polarizability of the heavy-alkali atoms [29] (inset in Fig. 1). The arrow in Fig. 1 indicates the position of a ${}^3F^o$ resonance we found for each system. This resonance will be discussed elsewhere.

Our Dirac R -matrix results for all three targets are shown in Tables I–V. Resonances are labeled in the jj - and LS -coupling schemes. The tables include the resonance positions E_r and widths Γ . In the low-lying spectrum of each negative ion, below the first np atomic threshold, we have identified the ${}^3P^o$ shape resonance and the ${}^3P^e$ Feshbach resonances [Tables I (Fr), II (Rb), and III (Cs)], and two ${}^1P_1^o$ autoionizing states (Table IV). A ${}^1D_2^o$ Feshbach resonance was identified below the second $np_{3/2}$ threshold for Cs ($n=6$) and Fr ($n=7$) targets, only. Tables I–V list the dominant configurations in the eigenvectors in terms of their

squared amplitude (only squared amplitudes larger than 3% are included).

With respect to the R -matrix poles, the matching conditions imposed on the two-electron wave function at the R -matrix sphere shift the position of all three fine-structure components of a given ${}^3L^\pi$ multiplet upward by approximately the same amount (e.g., for Rb: 2–3 meV for the ${}^3P^o$, and 1 meV for the ${}^3P^e$ resonance). None of the resonances is entirely characterized by just one configuration. Instead, we observe a distribution over the lowest configurations of a particular $nln'l'$ series defined by particular values of n , l , and l' quantum numbers. The fine-structure components of any particular ${}^3L^\pi$ resonance can be easily identified since the components of each ${}^3L^\pi$ multiplet are dominated by the same configurations. The fact that we can define a Landé constant A (see Tables I–III) for each resonance supports our correct identification of the resonances.

In this section we focus on resonances in $e^- + \text{Fr}$ scattering. Even though Fr was discovered 60 years ago [35] detailed information about its atomic spectrum has become available only very recently [28,32]. Its atomic and core polarizabilities were published two years ago [29]. The spectrum of Fr^- is very poorly known up to date, with no experimental data and only one previous calculation [27]. Based on the latest available spectroscopic data [28] and core polarizabilities for Fr [29,30], we have performed recently relativistic R -matrix calculations for electron scattering by Fr targets at energies below 120 meV [21], and provided a new value for the EA (492.46 meV). We have also analyzed the lowest ${}^3P^o$ resonance [21]. In the present electron scattering calculations, we focus on the ${}^3P^e$ and ${}^1D_2^o$ Feshbach reso-

TABLE II. As in Table I, but for electron scattering on Rb targets. We compare our calculations with electron-transmission spectroscopy data [6] and other calculations [38–40].

jj	J^π	Configurations (% probability)	E_k (meV)	E_r (meV)	Γ (meV)	${}^3L_J^\pi$ (Å)
$5snp$	0^-	$5s5p_{1/2}(31.9)$; $5s6p_{1/2}(37.8)$; $5s7p_{1/2}(25.7)$	17.17	19.21	14.84	${}^3P_0^o$
	1^-	$5s5p_{1/2}(20.5)$; $5s6p_{1/2}(25.4)$; $5s7p_{1/2}(17.9)$; $5s6p_{3/2}(13.5)$	18.43	20.42	18.24	${}^3P_1^o$
	2^-	$5s5p_{3/2}(29.1)$; $5s6p_{3/2}(38.1)$; $5s7p_{3/2}(28.2)$	20.89	23.22	20.89	${}^3P_2^o$
	J -av.	$5pn's(n' \geq 5)$		21.84 <50 [6] 13.6 [39] 39.0 [40]	19.33	${}^3P^o$ (1.3)
$5pnp$	0^+	$5p_{1/2}^2(40.5)$; $5p_{1/2}6p_{1/2}(24.0)$; $5p_{3/2}^2(18.3)$; $5p_{3/2}6p_{3/2}(9.4)$	1427.88	1428.99	0.002	${}^3P_0^e$
	1^+	$5p_{1/2}5p_{3/2}(58.9)$; $5p_{1/2}6p_{3/2}(17.7)$; $5p_{3/2}6p_{1/2}(15.6)$	1432.49	1433.45	0.026	${}^3P_1^e$
	2^+	$5p_{3/2}^2(40.2)$; $5p_{3/2}6p_{3/2}(21.6)$; $5p_{1/2}5p_{3/2}(19.0)$; $5p_{1/2}6p_{3/2}(6.2)$; $5p_{3/2}6p_{1/2}(5.3)$	1441.47	1442.37	0.34	${}^3P_2^e$
	J -av.	$5pn'p(n' \geq 5)$		1437.91 1435.2 [38] 1458.5 [39]	0.20	${}^3P^e$ (4.5)

TABLE III. As Table I, but for electron scattering by Cs targets, including the experimental data for photodetachment [16], and data for electron-transmission spectroscopy [10], and other quantum calculations [38–40].

jj	J^π	Configurations (% probability)	E_k (meV)	E_r (meV)	Γ (meV)	${}^3L_J^\pi$ (Å)
$6snp$	0^-	$6s6p_{1/2}(43.2)$; $6s7p_{1/2}(36.6)$; $6s8p_{1/2}(14.9)$	-1.37	1.69	0.36	${}^3P_0^o$
	1^-	$6s6p_{1/2}(27.4)$; $6s7p_{1/2}(25.5)$; $6s8p_{1/2}(11.5)$; $6s6p_{3/2}(13.2)$	3.09	5.53 8.0 [16]	2.67 5.0 [16]	${}^3P_1^o$
	2^-	$6s6p_{3/2}(35.5)$; $6s7p_{3/2}(39.1)$; $6s8p_{3/2}(20.8)$	11.05	12.74	8.73	${}^3P_2^o$
	J -av.	$6pn's(n' \geq 6)$		9.11 -12.2 [39] -1.0 [40]	5.78	${}^3P^o$ (3.7)
$6pnp$	0^+	$6p_{1/2}^2(43.3)$; $6p_{1/2}7p_{1/2}(23.2)$; $6p_{3/2}^2(16.8)$	1244.02	1244.66	0.03	${}^3P_0^e$
	1^+	$6p_{1/2}6p_{3/2}(60.3)$; $6p_{1/2}7p_{3/2}(17.1)$; $6p_{3/2}7p_{1/2}(12.3)$	1255.41	1256.31	0.16	${}^3P_1^e$
	2^+	$6p_{3/2}^2(45.5)$; $6p_{1/2}6p_{3/2}(13.5)$; $6p_{1/2}7p_{3/2}(6.2)$; $6p_{3/2}7p_{3/2}(18.8)$; $6p_{3/2}7p_{1/2}(5.3)$	1278.97	1278.05 1280 [10]	1.9	${}^3P_2^e$
	J -av.	$6pn'p(n' \geq 6)$		1267.50 1265.7 [38] 1069.4 [39]	1.10	${}^3P^e$ (11.1)

TABLE IV. Energies E_r , widths Γ , and associated eigenvectors (indicated by the dominant configurations) of the $^1P_1^o$ Feshbach resonances just below the np_j ($j=1/2$ and $3/2$) excitation thresholds in the 1^- symmetry for electron scattering by Rb ($n=5$), Cs ($n=6$), and Fr ($n=7$), including experimental data [12,13,15,17,18] and other theoretical results [27].

Target	Dominant configurations (% probability)	E_r (meV)		Γ (meV)	
		Our work	Others	Our work	Others
Rb	$5p_{1/2}6s(18.3)$; $5p_{1/2}7s(55.7)$; $5p_{1/2}8s(14.3)$	1559.60	1559.10 [12] 1559.48 [13] 1559.47 [18] 1559.60 [27]	0.14	0.15 [12] ~ 0.2 [13] 0.31 [18] ~ 0.1 [27]
		1589.06	— 1589.06 [27]	0.50	1.0 [12] ~ 0.9 [27]
		1385.93	1383.33 [12] 1383.58 [15] 1383.71 [17] 1385.69 [27]	0.40	1.0 [12] ~ 0.3 [15] ~ 1.8 [17] ~ 3 [27]
		1454.61	1454.01 [12] 1442.85 [15] 1452.76 [17] 1452.11 [27]	2.0	3.0 [12] ~ 9 [15] — ~ 6 [27]
Cs	$6p_{3/2}6s(20.3)$; $5p_{3/2}7s(51.5)$; $5p_{3/2}8s(12.3)$	1517.26	1517.26 [27]	0.07	$\ll 1$ [27]
		1726.02	1726.02 [27]	7.99	~ 6 [27]
		1726.02	1726.02 [27]	7.99	~ 6 [27]
Fr	$7p_{1/2}8s(19.5)$; $7p_{1/2}9s(60.6)$; $7p_{1/2}10s(12.3)$	1517.26	1517.26 [27]	0.07	$\ll 1$ [27]
		1726.02	1726.02 [27]	7.99	~ 6 [27]
		1726.02	1726.02 [27]	7.99	~ 6 [27]

nances of Fr^- and confirm the presence of the $^1P_1^o$ excited states below the $7p_{1/2}$ and $7p_{3/2}$ atomic thresholds predicted by Greene [27]. The characteristics of the resonances identified in the present relativistic R -matrix calculations are given in Tables I and IV. In order to demonstrate the level of accuracy of our calculations, we also present our similar calculations for $e^- + \text{Rb}$ (Tables II and IV) and Cs (Tables III and IV) collisions and compare them with other theoretical and experimental results.

A. $^3P^o$ and $^3P^e$ resonances of Fr^-

The R -matrix eigenvectors associated with the $^3P^o$ and $^3P^e$ resonances are mostly linear combinations of $7sn'p$ and $7pn'p$ configurations, respectively (Table I). The total contribution of these configurations is larger than 70% for all fine-structure components of both resonances such that both resonances are clearly dominated by p -wave scattering channels. The widths of the fine-structure components of the $^3P^o$ and $^3P^e$ resonances (Table I) increase with the total angular momentum J as for the case of the corresponding resonances

TABLE V. Energies E_r , widths Γ , and the associated eigenvectors (indicated by the dominant configurations) of the $^1D_2^o$ Feshbach resonances below the $np_{3/2}$ excitation thresholds in the 2^- symmetry for electron scattering on Cs ($n=6$) and Fr ($n=7$) targets.

Target	Dominant configurations (% probability)	E_k (meV)	E_r (meV)	Γ (meV)		
					Cs	$6sn'f_{5/2}(91.7)$ ($n'=4,5,6,7$); $6p_{1/2}n'd_{3/2}(5.1)$ ($n'=5,6,7$) $6p_{3/2}n's(87.6)$ ($n'=7,8,9$); $6p_{1/2}n'd_{5/2}(4.6)$ ($n'=6,7$)
$6p_{1/2}n'd_{3/2}(87.9)$ ($n'=5,6,7,8$); $5d_{3/2}n'p_{1/2}(5.6)$ ($n'=7,8$)	1475.71					
$7p_{1/2}n'd_{5/2}(94.7)$ ($n'=6,7,8,9$) $7p_{3/2}n's(85.7)$ ($n'=7,8,9$) $6d_{5/2}8p_j(6.6)$ ($j=1/2,3/2$) $7p_{1/2}n'd_{3/2}(72.5)$ ($n'=6,7,8,9$)	1626.30 1706.56 1712.60	1720.60	0.44			

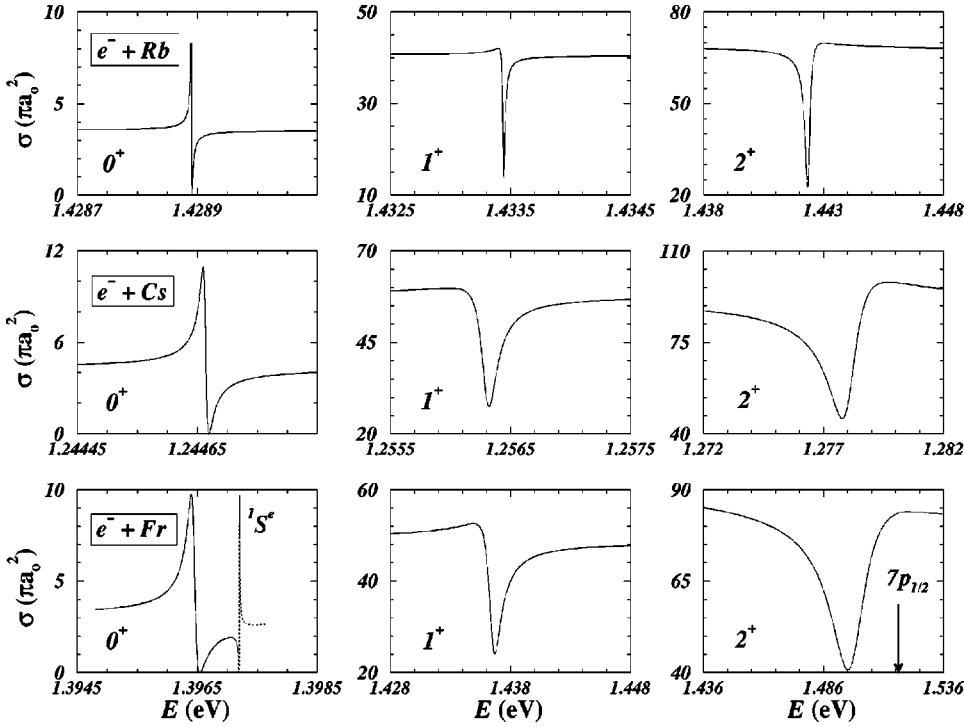


FIG. 2. The ${}^3P^e$ resonance in highly resolved partial elastic cross sections for electron scattering by Rb (top row), Cs (middle row), and Fr (bottom row) targets. The fine-structure components in the $J^\pi=0^+$, 1^+ , and 2^+ symmetries are shown. Also presented is a very narrow ${}^1S^e$ resonance of Fr^- (dotted curve). The arrow indicates the $7p_{1/2}$ atomic threshold of Fr.

of Rb^- (Table II) and Cs^- (Table III). We note that the width of neighboring ${}^3P_J^e$ terms of Fr^- increases by approximately an order of magnitude with increasing J , as for Rb^- and Cs^- .

We computed the J -averaged values for energy and width of triplet resonances according to

$$\bar{E} = \frac{\sum (2J+1)E_r(J)}{\sum (2J+1)} \quad (3.1)$$

and

$$\bar{\Gamma} = \frac{\sum (2J+1)\Gamma(J)}{\sum (2J+1)}. \quad (3.2)$$

The J -averaged width of the ${}^3P^0$ resonance (47.46 meV) is about five times larger than for the ${}^3P^e$ multiplet (9.89 meV).

Figures 2 and 3 show the profiles of the fine-structure components of the ${}^3P^e$ Feshbach resonance in highly resolved partial and total converged elastic cross section. The large difference (by a factor of 50) between the resonance widths for the lowest (${}^3P_0^e$) and the highest (${}^3P_2^e$) component (Table I) did not allow us to fully resolve the ${}^3P_0^e$ term in Fig. 3. Very close to the ${}^3P_0^e$ term, our calculation shows the presence of a very narrow ${}^1S^e$ resonance, which we did not observe in the vicinity of the ${}^3P_0^e$ resonance of Cs^- and Rb^- .

I. Comparison with ${}^3P^0$ and ${}^3P^e$ resonances of Rb^- and Cs^-

The ${}^3P_2^e$ term of the Fr^- (${}^3P^e$) resonance produces a minimum in the cross section at 19.45 meV below the $7p_{1/2}$ atomic threshold. This resonance has a large width (16.84 meV), such that its right wing extends beyond the $7p_{1/2}$ threshold (Fig. 2). The corresponding ${}^3P_2^e$ terms in Rb^- and Cs^- ions are located further below the lowest $np_{1/2}$ threshold, more than 100 meV in both cases [118 meV for Cs^- (${}^3P_2^e$) and 108 meV for Cs^- (${}^3P_2^e$)] and have a smaller width than in Fr^- . Therefore, the shape of the Rb^- (${}^3P_2^e$) and Cs^- (${}^3P_2^e$) terms is not affected by the opening of new (inelastic) scattering channels, in contrast to the Fr^- (${}^3P_2^e$) term. The ${}^3P^e$ excited state of Fr^- is a Feshbach resonance due to its dominant $7pn'p$ configuration and its position below the $7p_{1/2}$ threshold. Based on similar arguments, Rb^- (${}^3P^e$) and Cs^- (${}^3P^e$) are Feshbach resonances too.

Dirac R -matrix [24,25,36,37] and Breit-Pauli [26] calculations for electron-Cs scattering at energies below the $6p_{1/2}$ threshold were performed previously. The main difference with respect to these previous calculations is a larger number of continuum orbitals (28 per scattering channel instead of 24) in the present application and the use of the experimental (instead of calculated) atomic threshold energies.

Bartschat [26] has demonstrated the very high sensitivity of the Cs^- (${}^3P^e$) width to the details of the model. Our results for the Rb^- (${}^3P^e$) (Table II) and the Cs^- (${}^3P^e$) (Table III) resonances show that the dominant $npn'p$ configurations have a larger contribution for Rb (of 92%, $n=5$) than for Cs (of 83%, $n=6$). This supports the hypothesis that the interaction between the ${}^3P^e$ autoionizing state and the ionization continuum is more significant for Cs^- , which is confirmed by the smaller widths of all Rb^- (${}^3P^e$) terms. With respect to the previous results of Thumm and Norcross [24], we con-

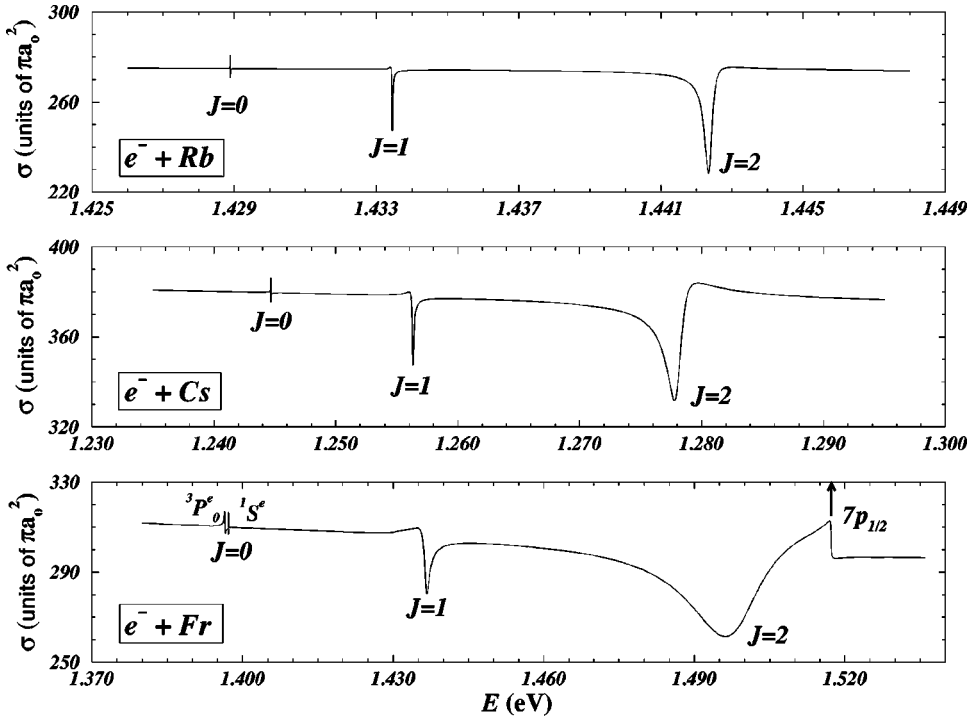


FIG. 3. The $J^\pi=0^+, 1^+,$ and 2^+ fine-structure components of the ${}^3P^e$ resonance in converged total elastic cross sections for electron scattering by Rb, Cs, and Fr targets. A very narrow ${}^1S^e$ resonance in Fr $^-$ occurs near the ${}^3P_0^e$ component.

firm the position of the ${}^3P^o$ and ${}^3P^e$ resonances, but find a significant correction for the widths of the ${}^3P_0^e$ term (we obtain $\Gamma=0.03$ meV compared to 0.009 meV [24]).

Apart from R -matrix calculations [21,24–27], various other theoretical models [20,22,23,38–41] were used to evaluate the J -averaged energy of the lowest ${}^3P^o$ and ${}^3P^e$ excited states of Rb $^-$ and Cs $^-$. All models predict that the even parity ${}^3P^e$ excited states of Rb $^-$ and Cs $^-$ are resonances embedded in the Rb $+e^-$ and Cs $+e^-$ continuum localized below the 2P atomic state (see Tables II and III). The energy of the highest ($J=2$) component of the Cs $^-$ (${}^3P^e$) identified in our relativistic R -matrix calculations (1278 meV) is in excellent agreement with electron scattering experiments [10] which found this component at about 1280 meV. This gives us confidence in our calculations. As far as we know, there is no clear experimental evidence for the ${}^3P^e$ resonances in the Rb $^-$ spectrum. The present experimental energy resolution in electron scattering of a few meV [42] seems to be insufficient for a definite identification of the ${}^3P^e$ resonance. In single-photon detachment experiments from the Rb $^-$ (${}^1S^e$) ground state, the ${}^3P^e$ excited state cannot be reached because the transition is forbidden by both spin and parity selection rules. The detection of the ${}^3P^e$ resonance may be difficult, because it can decay only due to relativistic effects and thus has an extremely narrow width (Table II).

The odd-parity ${}^3P^o$ excited state of Rb $^-$ was predicted by earlier calculations as an unbound state above the detachment threshold [20,39,40]. The bound or unbound character of the lowest ${}^3P^o$ excited state of Cs $^-$ was debated for a long time. Some theoretical computations indicated that the ${}^3P^o$ resonance is a bound state with respect to the detachment limit [20,27,39,40], while other works suggested a resonance state [21–26,41].

In Tables II and III, we compare our J -averaged calculations for the energy of ${}^3P^o$ and ${}^3P^e$ resonances of Rb $^-$ and Cs $^-$, respectively, with the available experimental results and other calculations. For Rb $^-$ and Cs $^-$ ions, our computed ${}^3P^o$ resonance energies are in agreement with the scattering experiment of Johnson and Burrow [6] (Table II), and the single-photon detachment experiment of Scheer *et al.* [16] (Table III).

Froese-Fischer and Chen [40] have performed multiconfiguration Hartree-Fock calculations for the ${}^3P^o$ excited state. A large number of configurations was included in their computations, and the energy of the resonance was corrected (by a few meV) for relativistic effects. Because of computational limitations, a limited number of configurations were included in Ref. [40]. However, a larger number seemed to be necessary since their convergence test for Rb $^-$ (${}^3P^o$) had shown that increasing the number of configurations from 734 to 850 shifts the resonance energy from 52 to 39 meV. For Cs $^-$, their ${}^3P^o$ excited state was found at 1 meV below the ground state of the Cs atom, i.e., to be bound. This result is in disagreement with very recent experimental data [16] and previous semiempirical calculations by Fabrikant [22].

Krause and Berry [39] have analyzed the distribution of probability of the two active electrons in the field of the Rb $^+$ and Cs $^+$ cores. For the Rb case, their computation shows that both the ${}^3P^o$ and ${}^3P^e$ excited states are resonances in the continuum of Rb(1S) $+e$, and are localized at 13.6 and 1458.5 meV, respectively, above the detachment limit. Our J -averaged energies \bar{E} for the ${}^3P^o$ and ${}^3P^e$ resonances differ from the results of Ref. [39] (Table II). Previously, Norcross [38] has performed nonrelativistic calculations using an effective model potential which included the same V_{diel} that we use in our calculations. He predicted the ${}^3P^e$ resonance of

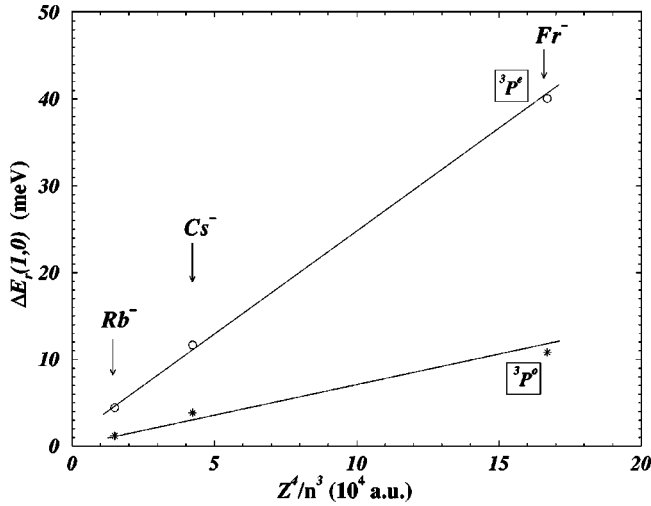


FIG. 4. The fine-structure splitting $\Delta E_r(1,0)$ between the $J=0$ and $J=1$ terms for the ${}^3P^o$ and ${}^3P^e$ resonances vs Z^4/n^3 . Z is the nuclear charge; n is the principal quantum number of the dominant $nl\ n'l'$ configurations ($n=5$ for Rb, 6 for Cs, and 7 for Fr).

Rb^- at about 144 meV below the $5p$ atomic excitation threshold (of 1579.24 meV). This result is in excellent agreement with our present relativistic calculations. The difference between the position of the ${}^3P^o$ and ${}^3P^e$ resonances predicted by Krause and Berry [39] and the present results could be attributed to the lack of the V_{diel} term in Ref. [39]. Krause and Berry have used the pseudopotentials proposed by Bachelet, Hamann, and Schlüter [43] even though Norcross [38] had already pointed to the importance of the V_{diel} term in shifting upward the positions of the ${}^3P^e$ resonance for alkali-negative ions.

For Cs, the calculations of Krause and Berry [39] have predicted the ${}^3P^o$ state as bound at 12.2 meV, below the

detachment limit of Cs^- (Table III). They have predicted the ${}^3P^e$ excited states at about 1069.4 meV (Table III) above the detachment limit. Their result differs by 15.6% from our J -averaged value of 1267.5 meV for the ${}^3P^e$ resonance. As for the Rb^- (${}^3P^e$) resonance, the difference between the calculations in Ref. [39] and the present calculations could be attributed to the lack of the dielectronic polarization correction in the electrostatic potential used in Ref. [39]. The earlier nonrelativistic calculations of Norcross [38] predicted the ${}^3P^e$ resonance at 1265.7 meV, which is almost identical with our result (1267.5 meV).

The Landé constant A is a measure of the strength of spin-orbit interaction (Tables I–III). We find that A is more than three times larger for ${}^3P^e$ than for ${}^3P^o$ resonances, in all cases. Also, our calculations reveal that for both resonances A is proportional to Z^4/n^3 from Rb^- to Fr^- (Fig. 4). Z is the nuclear charge and n is the principal quantum that characterizes the dominant $nl\ n'l'$ configurations ($n=5$ for Rb, 6 for Cs, and 7 for Fr). As expected, the spin-orbit interaction (which approximately varies as Z^4/n^3) is more significant for Fr^- than for Cs^- and Rb^- .

B. ${}^1P_1^o$ resonance of Fr^-

In the $J^\pi=1^-$ symmetry, below the $7p_j$ excitation thresholds, we find two ${}^1P_1^o$ Feshbach resonances, which are characterized by the same $7p\ n's$ configurations in the s -wave scattering channel (Table IV). In Fig. 5, we show the shape of ${}^1P_1^o$ resonances in the converged total elastic cross section in a small energy range around the $7p_{1/2}$ and $7p_{3/2}$ thresholds. The ${}^1P_1^o$ resonance located below the $7p_{1/2}$ atomic threshold is narrower than the corresponding resonance for Rb^- and Cs^- (Table IV), while the ${}^1P_1^o$ resonance located below the second atomic excitation threshold is broader by a

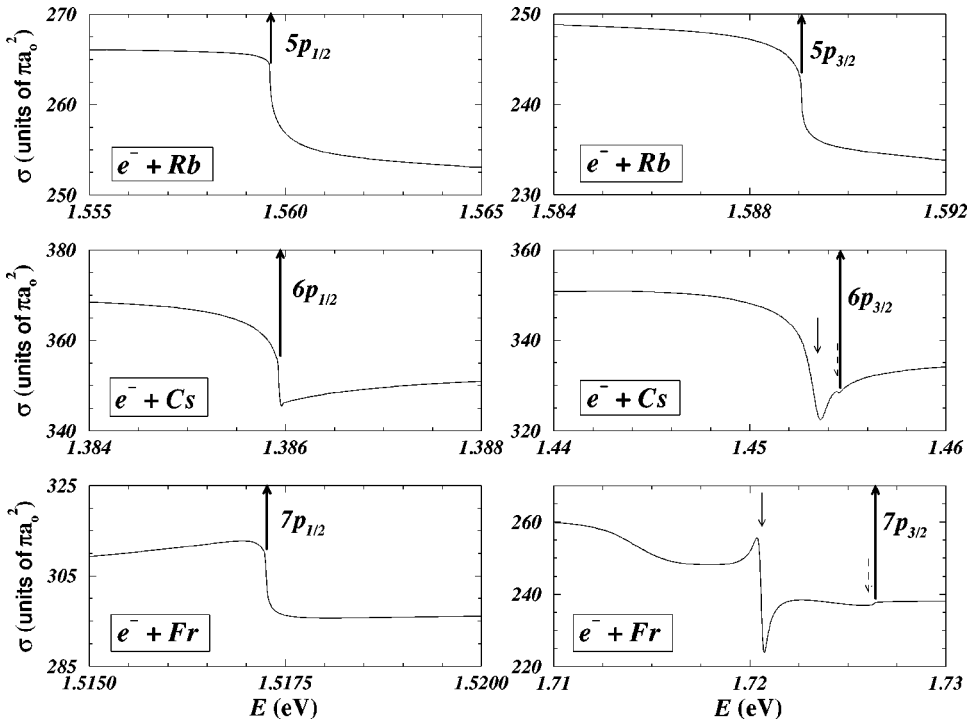


FIG. 5. Highly resolved total converged cross sections for elastic electron scattering by Rb, Cs, and Fr targets, near the first atomic excitation thresholds np_j (where $j=1/2, 3/2$, and $n=5$ for Rb, 6 for Cs, and 7 for Fr) indicated by a thick solid arrow. The ${}^1P_1^o$ and ${}^1D_2^o$ Feshbach states of Cs^- and Fr^- near the $np_{3/2}$ threshold are indicated by a thin dashed and solid arrow, respectively.

factor of 4 (16) than the corresponding resonance in Cs^- (Rb^-).

The calculation of Greene [27] for the photoabsorption spectrum of Fr^- indicated the presence of two $^1P_1^o$ states with minima at the $7p_{1/2}$ threshold (at 1517.26 meV) and at 0.35 meV below the $7p_{3/2}$ threshold, in excellent agreement with our calculation (Table IV).

Due to the strong variation of the background phase shift Δ_0 for collision energies in the neighborhood of the excitation threshold, accurate resonance widths Γ cannot be computed from the eigenphase sums Eq. (2.1). Therefore we estimate the widths of the $^1P_1^o$ states from the full width half maximum (FWHM) of the partial elastic cross section. For the $^1P_1^o$ resonances of Rb^- and Cs^- , such an estimation of Γ gives smaller values than the measured data (see Table IV).

1. Comparison with $^1P_1^o$ resonance of Rb^-

The $^1P_1^o$ resonances located just below the $5p_{1/2}^2P_{1/2}$ and $5p_{3/2}^2P_{3/2}$ excitation thresholds of Rb are well known from various independent measurements using single- or multiphoton detachment techniques [12–14,18]. The first measurement of single-photon detachment from Rb^- was performed by Patterson and co-workers [12] by using a hot-cathode discharge source to produce alkali-metal negative ions. Afterwards, more sophisticated crossed ion-laser beam experiments [13–15] were realized and have confirmed the previous measurements of Patterson *et al.* The high energy resolution in the detachment experiments (0.012 meV) of Frey, Beyer, and Hotop [13] allowed to discriminate between the cusp at the $5p_{1/2}$ threshold and the $^1P_1^o$ Feshbach resonance. Very recently a new multiphoton detachment experiment in a strong laser field was done in Aarhus [18] which demonstrated that photoabsorption in Rb^- is strongly enhanced when the first photon reaches an energy that coincides with the $^1P_1^o$ excited state. In these experiments, very narrow $^1P_1^o$ resonances with *window*-like shapes were identified just below the first $5p_j$ ($j=1/2$ and $3/2$) atomic excitation thresholds of Rb. The energy E_r and width Γ of these two $^1P_1^o$ resonances measured in both single and excess-photon detachment experiments are given in Table IV in comparison with our relativistic *R*-matrix calculations for electron scattering. Patterson *et al.* [12] have identified a narrow resonance with the minimum at 0.5 ± 3 meV below the $5p_{1/2}$ threshold. In later experiments, Frey, Beyer, and Hotop [13] and Stapelfeldt *et al.* [18] found the minimum of the $^1P_1^o$ state at about 0.13 meV below the $5p_{1/2}$ threshold (Table IV). The absolute error in energy in [13] is ± 0.012 meV. We have estimated a width of 0.2 meV from the photodetachment cross section given in Fig. 2 of Ref. [13] (Table IV).

To date, the only calculations for these $^1P_1^o$ resonances of Rb^- were performed by Greene [27], who found evidence in the photoabsorption spectrum for very narrow states just below the two $5p_j$ atomic thresholds of Rb. However, compared with the experimental signal [13], Greene's $^1P_1^o$ states are narrower and their minima coincide with the position of the $5p_j$ thresholds (Fig. 5 in [27]). We find two narrow fea-

tures in the elastic scattering channel just below the $5p_j$ thresholds which can be labeled in the *LS*-coupling scheme as $^1P_1^o$ states, due to the large contribution to the associated eigenvector of the $5p_j n's$ configurations (Table III). We agree with Greene's result in the sense that the minima of the two Feshbach states are located exactly at the $5p_j$ thresholds and therefore, the calculations indicate the $^1P_1^o$ features as virtual states, rather than Feshbach resonances. The strong dominance of the $5p_j n's$ configurations suggests that the $^1P_1^o$ state is produced in a *s*-wave scattering channel.

Our scattering calculation in the 1^- symmetry fails to reproduce the *window* profile of the $^1P_1^o$ resonances observed experimentally [13], in contrast to the calculation of Greene [27]. The result of Greene (see Fig. 5(b) in [27]) shows a significant contribution of inelastic cross sections to the total cross section in the 1^- symmetry, while in our calculation the inelastic cross section has a weak contribution.

We note that Stapelfeldt *et al.* [18] label the autoionizing state located below the $5p_{1/2}$ threshold by a single dominant configuration, $5p_{1/2}6s$. Our calculation indicates that the $5p_{1/2}7s$ configuration largely dominates (with 55.7%) the eigenvector associated with this state, and the label “ $5p_{1/2}7s$ ” seems to be more appropriate than “ $5p_{1/2}6s$.” Nevertheless, we prefer to use a general label $5p_{1/2}n's$, to indicate the strong admixture of several configurations. We found no other resonance between the $5p_{1/2}$ and $5p_{3/2}$ thresholds in the 1^- symmetry.

2. Comparison with $^1P_1^o$ resonances of Cs^-

Single- and multiphoton detachment experiments [12,15,17] similar to those done on Rb^- were performed on Cs^- and have indicated the presence of two $^1P_1^o$ Feshbach resonances just below the $6p_{1/2}^2P_{1/2}$ and $6p_{3/2}^2P_{3/2}$ excitation thresholds. Figure 5 shows the converged *total* elastic cross section in a small range of energies around the $6p_{1/2}$ and $6p_{3/2}$ thresholds. The two $^1P_1^o$ autoionizing states have a similar shape in the elastic scattering channel, but a larger width than those observed in Rb^- . Compared with Rb^- , the total cross section in the 1^- symmetry for Cs^- obtains a more significant contribution from the inelastic channels above each threshold. Table IV shows our results for the energies and widths of the $^1P_1^o$ resonances, together with the available experimental data. We locate one $^1P_1^o$ resonance at 0.01 meV below the $6p_{1/2}$ threshold and the second one at 0.02 meV below the $6p_{3/2}$ threshold. Patterson *et al.* [12] have found two resonances at 2.6 and 0.6 meV (with an error of ± 3 meV) below the $6p_{1/2}$ and $6p_{3/2}$ thresholds, respectively. Their widths are larger than ours (Table IV). The presence of the $^1P_1^o$ resonance below the $6p_{1/2}$ threshold was confirmed later experimentally, by Slater *et al.* [15] and by Stapelfeldt and Haugen [17], but different values of Γ were found (Table IV). The position of the $^1P_1^o$ Feshbach resonance below the $6p_{3/2}$ threshold was found at different energies in Refs. [12,15,17]: in Ref. [15] the minimum of the resonance is located at 11.8 meV below the $6p_{3/2}$ threshold, while in Ref. [17] a very broad structure was identified at 1.9 meV below this threshold (Table IV). From the experimental

data in Ref. [15], we estimated widths of the two $^1P_1^o$ resonances of 0.3 and 9 meV, while in Ref. [17] the width of the $^1P_1^o$ resonance below the $6p_{1/2}$ threshold is given as 1.8 meV. For both resonances, our values for Γ are smaller than the experimental data. We cannot confirm the labels used for the $^1P_1^o$ resonances in the jj -coupling scheme by Stapelfeldt and Haugen [17]: $6p_{1/2} 7s$ and $6p_{3/2} 7s$. Our calculations indicate a strong admixture of $6p_j n's$ configurations, dominated by the $6p_j 8s$ configuration. Both the dominance of the $6p_j n's$ configurations and the location below the $6p_j$ threshold justify the label “*Feshbach resonance*” for the two $^1P_1^o$ states.

Previous theoretical studies of the low-energy photoabsorption spectrum of Cs⁻ (Fig. 4 in Ref. [27]) indicate the presence of two $^1P_1^o$ resonances at 0.25 and 2.5 meV below the $6p_{1/2}$ and $6p_{3/2}$ atomic thresholds, respectively (Table IV). Their widths are larger than our results. As for the Rb⁻ ($^1P_1^o$) resonances discussed in the previous section, a possible reason for this discrepancy is the different number of scattering channels included in the two different calculations.

C. $^1D_2^o$ resonance of Fr⁻

In the $J^\pi=2^-$ symmetry, at about 5.8 meV below the $7p_{3/2}$ excitation threshold, we find a resonance which is easily identified as a jump of approximately π in the eigenphase sum. Its eigenvector is largely dominated by the same $7p n's$ configurations (about 85.7%), as the two $^1P_1^o$ resonances. A weak contribution (of 6.6%) is due to the $6d_{5/2} 8p_j$ configurations (Table V). In order to find the appropriate label in the jj - and LS -coupling schemes, we have analyzed the contribution of dominant configurations for the three R -matrix poles in Table V. These are the closest poles to the $7p_{3/2}$ threshold. Our calculations without the $7p_{1/2} n'd_{5/2}$ and $7p_{1/2} n'd_{3/2}$ configurations, which dominate the eigenvectors $E_k=1626.30$ meV and 1712.60 meV (Table V), respectively, do not modify the characteristics (position and shape) of the resonance below $7p_{3/2}$ threshold and change only the background. When each of the dominant $7p_{3/2} n's$ and $6d_{5/2} 8p_j$ configurations of the eigenvector associated to the pole $E_k=1706.56$ meV is left out, the resonance feature below the $7p_{3/2}$ threshold in 2^- symmetry disappears. When the $7p_{3/2} n's$ configuration is left out, both the threshold effect at and the resonance feature below the $7p_{3/2}$ threshold disappear. In jj coupling, the $7p_{3/2} n's$ and $np_j n'd_{j'}$ (with $n=7$ and 8) configurations may contribute to this resonance.

The relevance of the $7p_{3/2} n's$ configurations may suggest that the feature below the $7p_{3/2}$ threshold in the 2^- symmetry is a 3P resonance, while the $6d_{5/2} 8p_j$ configurations might support either a triplet P , D , or F resonance, or a singlet D resonance. However, we did not find a triplet resonance in the 0^- , 1^- , 3^- , and 4^- symmetries near the $7p_{3/2}$ threshold. Therefore, in the LS -coupling scheme, the resonance symmetry appears to be $^1D_2^o$, which is somewhat surprising in view of the weak (6.6%) contribution of the $6d_{5/2} 8p_j$ configurations. A general label “ $^1X_2^o$ ” might be more appropriate and allows for the admixture of P and D

total orbital momenta. This ambiguity in finding the label in the LS -coupling scheme favors the jj -coupling scheme. Nevertheless, in the following we prefer to use the label $^1D_2^o$ for convenience. The dominant $7p_{3/2} n's$ configuration and its position below the $7p_{3/2}$ threshold indicates that the $^1D_2^o$ state is a Feshbach resonance.

The Buttle correction [33] strongly modifies the characteristics of the $^1D_2^o$ resonance. The omission of this correction shifts the resonance energy by 3.3 meV. This reveals the strong influence of high-lying configurations. Therefore, the contribution of the particular configurations listed in Table V should be regarded with some precautions.

The structure in the converged *total* elastic cross section (Fig. 5) just below the $7p_{1/2}$ threshold is due solely to the $^1P_1^o$ resonance in the 1^- symmetry. Just below the $7p_{3/2}$ threshold, the structure in the converged *total* elastic cross section results from the overlap between the $^1P_1^o$ and $^1D_2^o$ resonances.

1. Comparison with $^1D_2^o$ resonances of Cs⁻

Our relativistic calculation indicates a new resonance in the 2^- symmetry at about 1 meV below the $6p_{3/2}$ threshold of Cs (Table V). The eigenvector associated with this resonance is largely dominated by the same $6p n's$ configuration (about 87.6%, see Table V), as for the two $^1P_1^o$ resonances (Table III). In Table V, we give the poles and eigenvectors (indicated by the configurations with a contribution larger than 3%) located near and below the $6p_{3/2}$ threshold (1454.63 meV). A similar study to the Fr⁻ ($^1D_2^o$) resonance discussed in the previous section was done for the $^1D_2^o$ resonance of Cs⁻. We performed calculations without the dominant configurations that belong to $E_k=1170.31$ and 1475.71 meV poles (Table V). Similar arguments to those provided for the Fr⁻ ($^1D_2^o$) resonance suggest that the feature below the $6p_{3/2}$ threshold in the 2^- symmetry is a $^1D_2^o$ resonance but, again, a general $^1X_2^o$ label might be more appropriate.

With respect to the Fr⁻ ($^1D_2^o$) resonance, for the Cs⁻ ($^1D_2^o$) resonance the $np_j n'd_{j'}$ configurations give a smaller contribution. The width of the Cs⁻ ($^1D_2^o$) resonance is twice as large as that for Fr⁻ ($^1D_2^o$) (Table V). The resonance feature, which we have observed at the same energy but in the $6s \rightarrow 6p_{1/2}$ inelastic channel, is supported by contributions from the $6p_{1/2} n'd_{5/2}$ configurations. As far as we know, this resonance was never observed in experiments. Using the single-photon detachment technique, the $^1D_2^o$ excited state cannot be reached by photoabsorption from the ground state of the negative ion.

As for Fr⁻, the $^1P_1^o$ and $^1D_2^o$ resonances overlap in the *total* converged cross section (Fig. 5), but for Cs⁻, the two states are much closer, and in consequence harder to distinguish.

D. Discussion and summary

At a first glance, the spectrum of Fr⁻ looks very similar to that of Rb⁻ and Cs⁻. The resonances in Fr⁻ are in general much broader than the corresponding resonances in Rb⁻ and Cs⁻, except for the $^3P_0^o$ resonance which is broader in Rb⁻. The contribution of the dominant configurations to the eigenvectors associated with the low-lying resonances of Fr⁻ is

similar for Rb^- and Cs^- ions. The spin-orbit interaction is stronger in Fr^- than in Rb^- and Cs^- , leading to larger values for the Landé constant A , i.e., larger splitting between the fine-structure components.

Except for the $^1D_2^o$ Feshbach resonance found in scattering calculations for Cs and Fr targets, all other resonances simultaneously occur in the low-lying spectra of the three heavy-alkali negative ions investigated here. Our calculations also show that the fine-structure components of a given $^3P^\pi$ term on different negative ions have very similar profiles and almost the same Fano-asymmetry parameter q .

For hydrogenic ions, the fine-structure splitting $\Delta E_r(J, J-1)$ between adjacent levels increases with Z^4/n^3 , where n is the principal quantum number [34]. This also applies to the low-lying resonances of the heavy-alkali negative ions located below the first atomic threshold $np_{1/2}$. Figure 4 shows the linear dependence of the energy splitting $\Delta E_r(1,0)$ between the $J=0$ and $J=1$ terms and for the $^3P^o$ and $^3P^e$ resonance as a function of Z^4/n^3 , where n is the principal quantum number which defines the dominant $nl\ n'l'$ configurations (Tables I–III).

Our relativistic calculations for the $^3P^o$ and $^3P^e$ resonances identified in the low-lying spectra of Rb^- and Cs^- are in excellent agreement with the experimental results, whereas for the $^1P_1^o$ autoionizing states located just below the first atomic threshold, neither our computations, nor previous photodetachment calculations [27] find the same resonance position as the photodetachment measurements on Rb^- [12–14,18] and Cs^- [12,15,17] (Table IV). In particular, both calculations find the minimum of the $\text{Rb}^-(^1P_1^o)$ excited state on the $5p_{1/2}$ atomic threshold, while very precise experiments [13] found it at 0.13 ± 0.012 meV below this threshold (Table IV). Therefore, in our calculations these two $^1P_1^o$ excited states appear as *virtual states*, rather than Feshbach resonances. In order to reproduce resonances so close to the atomic thresholds, the theoretical calculation should be done with an accuracy of $10\ \mu\text{eV}$. As far as we know, nobody has reached such high accuracy in computations of the negative ion spectra up to now. Our calculations reproduce the measured positions of the fine-structure terms of triplet resonances within the experimental error in the resonance energy of 1 meV. This precision was obtained in accurate electron scattering experiments for the $\text{Cs}^-(^3P_2^e)$ resonance [10] and is exceeded in photodetachment experiments for the $^3P_1^o$ autoionizing state of Cs^- [16] (Table III). The difference in accuracy between our calculations of triplet resonances and the $^1P_1^o$ autoionizing states can be explained in terms of the spatial symmetry of singlet and triplet states as follows.

The Pauli exclusion principle requires the spatial wave function of the singlet state to be symmetric, while a triplet state has an antisymmetric spatial wave function. An antisymmetric spatial wave function tends to keep the two active electrons away from each other. Therefore, for singlet resonances the short-range electronic correlations are more important than for triplet resonances. For the same reason, long-range interelectronic couplings, such as V_{diel} , are more influential in triplet resonances. Thumm and Norcross [24]

have carefully analyzed the influence of long-range potentials and have shown that the inclusion of V_{diel} shifts the $\text{Cs}^-(^3P^o)$ bound excited state by about 25 meV into the continuum [24]. Their predictions for the low-lying $^3P^o$ states were confirmed by recent experiments [16].

Our tests with and without the V_{diel} term included in the total Hamiltonian confirm the assumption that the symmetric spatial wave function of a singlet resonance is weakly affected by the long-range potential V_{diel} . In order to accurately describe the $^1P_1^o$ resonances located below 1 meV from the atomic threshold, short-range electronic correlations are important and more scattering channels need to be included than for triplet states. The experimental evidence shows that the $^1P_1^o$ resonance is located much closer to the first $np_{1/2}$ threshold for Rb^- (a few hundred μeV below the $5p_{1/2}$ threshold) than for Cs^- (a few meV below $6p_{1/2}$ threshold). Since both our calculations and experiments suggest the $\text{Rb}^-(^1P_1^o)$ resonance to be very close to or on the $5p_{1/2}$ threshold, we expect our results for the $\text{Cs}^-(^1P_1^o)$ resonance to be more reliable. In future calculations, more bound states (i.e., more closed scattering channels) need to be included in order to characterize with higher accuracy all $^1P^o$ Feshbach resonances reported here.

IV. CONCLUSION

We have calculated the low-lying spectra of Rb^- , Cs^- , and Fr^- ions by analyzing electron-atom scattering cross sections at collision energies below 2.8 eV. Our calculations are based on the relativistic R -matrix code of Thumm and Norcross [24]. A number of autoionizing states ($^3P^o$, $^3P^e$, and $^1P_1^o$) were identified in the spectra of all three negative ions. For Cs and Fr targets, our calculation indicates the presence of a new $^1D_2^o$ resonance at a few meV below the lowest $np_{3/2}$ atomic excitation threshold. Our electron scattering calculations agree well with available experimental data for Rb and Cs and with other calculations. As far as we know, this is the first electron-scattering calculation for Fr targets. We hope that the present results will stimulate further experimental studies (either multiphoton detachment or electron scattering) on heavy-alkali negative ions. By using photoelectrons emitted by synchrotron radiation [42], an energy resolution below 3.5 meV (FWHM) for electrons with kinetic energies between 0.01 and 10 eV has recently been achieved in electron-transmission experiments. Very recently, Cavalieri and Eramo [44] have proposed an alternative method which is currently being used for single-photon spectroscopy of high-lying autoionizing states. This new time-delay spectroscopy approach could be a useful tool for the study of autoionizing states with short laser pulses.

ACKNOWLEDGMENTS

This work is supported by the Science Division, Office of Fusion Energy Sciences, Office of Energy Research, U.S. Department of Energy. One of us (U.T.) acknowledges the hospitality of the Institute for Theoretical Atomic and Molecular Physics at Harvard University and the Smithsonian Astrophysical Observatory, while this work was in progress.

- [1] G.J. Schulz, *Rev. Mod. Phys.* **45**, 378 (1973).
- [2] T. Andersen, *Phys. Scr.*, T **34**, 23 (1991).
- [3] S.J. Buckman and Ch.W. Clark, *Rev. Mod. Phys.* **66**, 539 (1994).
- [4] C. Blondel, *Phys. Scr.*, T **58**, 31 (1995).
- [5] H. Hotop and W.C. Lineberger, *J. Phys. Chem. Ref. Data* **28**, 1511 (1999).
- [6] A.R. Johnson and P.D. Burrow, *J. Phys. B* **15**, L745 (1982).
- [7] A.R. Johnson and P.D. Burrow, *Phys. Rev. A* **51**, 406 (1995).
- [8] P.J. Visconti, J.A. Slevin, and K. Rubin, *Phys. Rev. A* **3**, 1310 (1971).
- [9] B. Jaduszliwer and Y.C. Chan, *Phys. Rev. A* **45**, 197 (1992).
- [10] K. Bartschat, A.R. Johnson, and P.D. Burrow, *J. Phys. B* **27**, L231 (1993).
- [11] W. Gehenn and E. Reichert, *J. Phys. B* **10**, 3105 (1977).
- [12] T.A. Patterson, H. Hotop, A. Kasdan, D.W. Norcross, and W.C. Lineberger, *Phys. Rev. Lett.* **32**, 189 (1974).
- [13] P. Frey, F. Breyer, and H. Hotop, *J. Phys. B* **11**, L589 (1978).
- [14] N. Rouze and R. Geballe, *Phys. Rev. A* **27**, 3071 (1983).
- [15] J. Slater, F.H. Read, S.E. Novick, and W.C. Lineberger, *Phys. Rev. A* **17**, 201 (1978).
- [16] M. Scheer, J. Thogersen, R.C. Bilodeau, C.A. Brodie, H.K. Haugen, H.H. Andersen, P. Kristensen, and T. Andersen, *Phys. Rev. Lett.* **80**, 684 (1998).
- [17] H. Stapelfeldt and H.K. Haugen, *Phys. Rev. Lett.* **69**, 2638 (1992).
- [18] H. Stapelfeldt, P. Kristensen, U. Ljungblad, T. Andersen, and H.K. Haugen, *Phys. Rev. A* **50**, 1618 (1994).
- [19] I. I. Fabrikant, *Phys. Lett.* **58A**, 21 (1976).
- [20] I.I. Fabrikant, *Opt. Spektrosk.* **53**, 223 (1982) [*Opt. Spectrosc.* **53**, 131 (1982)].
- [21] C. Bahrim and U. Thumm, *Phys. Rev. A* **61**, 022722 (2000).
- [22] I.I. Fabrikant, *J. Phys. B* **19**, 1527 (1986).
- [23] V.M. Borodin, I.I. Fabrikant, and A.K. Kazansky, *Phys. Rev. A* **44**, 5725 (1991).
- [24] U. Thumm and D.W. Norcross, *Phys. Rev. Lett.* **67**, 3495 (1991); *Phys. Rev. A* **45**, 6349 (1992).
- [25] U. Thumm and D.W. Norcross, *Phys. Rev. A* **47**, 305 (1993).
- [26] K. Bartschat, *J. Phys. B* **26**, 3595 (1993).
- [27] C.H. Greene, *Phys. Rev. A* **42**, 1405 (1990).
- [28] E. Biemont, P. Quinet, and V. Van Renterghem, *J. Phys. B* **31**, 5301 (1998).
- [29] A. Derevianko, W.R. Johnson, M.S. Safronova, and J.F. Babb, *Phys. Rev. Lett.* **82**, 3589 (1999).
- [30] W. R. Johnson and A. Derevianko, (private communication).
- [31] C. E. Moore, *Atomic Energy Levels*, National Bureau Standards (U.S.) NSRDS-NBS 35, Vols. II and III (U.S. GPO, Washington, D.C., 1971).
- [32] E. Arnold, W. Borchers, H.T. Duong, P. Jumcar, J. Lerme, P. Lievens, W. Neu, R. Neugart, M. Pellarin, J.L. Vialle, K. Wendt, and ISOLDE Collaboration, *J. Phys. B* **23**, 3511 (1990); J.E. Simsarian, A. Ghosh, G. Gwinner, L.A. Orozco, G.D. Sprouse, and P.A. Voytas, *Opt. Lett.* **21**, 1939 (1996).
- [33] P.J.A. Buttle, *Phys. Rev.* **160**, 719 (1967).
- [34] B. H. Bransden and C. J. Joachain, *Physics of Atoms and Molecules* (Longman Scientific & Technical, New York, 1994).
- [35] M. Perey, *C. R. Hebd. Seances Acad. Sci.* **208**, 97 (1939).
- [36] K. Bartschat, U. Thumm, and D.W. Norcross, *J. Phys. B* **25**, L641 (1992).
- [37] U. Thumm, K. Bartschat, and D.W. Norcross, *J. Phys. B* **26**, 1587 (1993).
- [38] D.W. Norcross, *Phys. Rev. Lett.* **32**, 192 (1974).
- [39] J.L. Krause and R.S. Berry, *Comments At. Mol. Phys.* (We refer in Table II (for Rb) and III (for Cs) to the calculated ionization potentials in this reference.) **18**, 91 (1986).
- [40] C. Froese-Fischer and C. Chen, *J. Mol. Struct.: THEOCHEM* **199**, 61 (1989).
- [41] I.I. Fabrikant, *Comments At. Mol. Phys.* **32**, 267 (1996).
- [42] S.L. Lunt, D. Field, S.V. Hoffmann, R.J. Gulley, and J.-P. Ziesel, *J. Phys. B* **32**, 2707 (1999); **31**, 5197 (1998).
- [43] G.B. Bachelet, D.R. Hamann, and M. Schlüter, *Phys. Rev. B* **26**, 4199 (1982).
- [44] S. Cavalieri and R. Eramo, *Phys. Rev. A* **58**, R4263 (1999).